Dynamic interference of two anti-phase flapping foils in side-by-side arrangement in an incompressible flow

Cite as: Phys. Fluids **29**, 033601 (2017); https://doi.org/10.1063/1.4978301
Submitted: 15 September 2016 . Accepted: 23 February 2017 . Published Online: 17 March 2017

Y. Bao, D. Zhou, J. J. Tao, Z. Peng, H. B. Zhu, Z. L. Sun, and H. L. Tong

Dynamic interference of two anti-phase flapping foils in side-by-side arrangement in an incompressible flow

Y. Bao,[1,2,a)] D. Zhou,[1,2,3] J. J. Tao,[4] Z. Peng,[5] H. B. Zhu,[1] Z. L. Sun,[4] and H. L. Tong[6]
[1]*Department of Civil Engineering, School of Naval Architecture, Ocean and Civil Engineering, Shanghai Jiaotong University, Shanghai 200240, China*
[2]*State Key Laboratory of Ocean Engineering, Shanghai Jiaotong University, Shanghai 200240, China*
[3]*Collaborative Innovation Center for Advanced Ship and Deep-Sea Exploration, Shanghai 200240, China*
[4]*CAPT and SKLTCS, Department of Mechanics and Aerospace Engineering, College of Engineering, Peking University, Beijing 100871, China*
[5]*Department of Aerospace and Mechanical Engineering, University of Notre Dame, Notre Dame, Indiana 46556, USA*
[6]*Inner Mongolia Vocational College of Chemical Engineering, Huhhot 010070, China*

(Received 15 September 2016; accepted 23 February 2017; published online 17 March 2017)

A two-dimensional computational hydrodynamic model is developed to investigate the propulsive performance of a flapping foil system in viscous incompressible flows, which consists of two anti-phase flapping foils in side-by-side arrangement. In the simulations, the gap between the two foils is varied from 1.0 to 4.0 times of the diameter of the semi-circular leading edge; the amplitude-based Strouhal number is changed from 0.06 to 0.55. The simulations therefore cover the flow regimes from negligible to strong interference in the wake flow. The generations of drag and thrust are investigated as well. The numerical results reveal that the counter-phase flapping motion significantly changes the hydrodynamic force generation and associated propulsive wake. Furthermore, the wake interference becomes important for the case with a smaller foil-foil gap and induces the inverted Bénard von Kármán vortex streets. The results show that the hydrodynamic performance of two anti-phase flapping foils can be significantly different from an isolated pitching foil. Findings of this study are expected to provide new insight for developing hydrodynamic propulsive systems by improving the performance based on the foil-foil interaction. *Published by AIP Publishing.* [http://dx.doi.org/10.1063/1.4978301]

I. INTRODUCTION

In nature, the locomotion of many swimming species through a fluid medium is usually achieved by making flapping and pitching motions of their appendages such as tails and fins. Besides employing flapping-based techniques to produce propulsive and lifting forces, many aquatic creatures also extract energy from the ambient flow environment to reduce their own energy consumption in locomotion. For example, groups of fish take advantage of the adjacent vortices shed by neighbors to increase efficiency in swimming.[39] However, for such biological schooling system, the fundamental mechanism is still not well understood or characterized for concerning their high locomotion efficiency. This is also important for developing bio-inspired autonomous underwater vehicles (AUVs), particularly those operated in groups. In this study, the hydrodynamics of a simplified model of two side-by-side flapping hydrofoils in proximate arrangement are numerically examined. It will be expected to improve the knowledge of the basic physical mechanism of efficient propulsion and maneuvering forces through flow interference.

Unsteady propulsion by hydrofoils was identified both experimentally[2] and computationally.[29] Anderson *et al.*[2] found that a foil in harmonic heaving and pitching motion produces thrust through the formation of momentum jet (in the sense of flow average) downstream from the trailing edge. They further reported that high propulsive efficiency, as high as 87%, is achieved for oscillating foils as the formation of inverted Bénard von Kármán (BvK) street in the wake is under the interactions of a moderately strong leading-edge vortex and trailing-edge vorticity. The phase angle between transverse oscillation and angular motion is also found to be the critical parameter affecting the efficiency of propulsion. In the numerical investigation in Lewin and Haj-Hariri,[29] effects of the interaction of leading edge and trailing edge vortices on the propulsive efficiency were discussed. Their results showed that the greatest efficiency occurs for the proximity of the heaving frequency to the frequency of the most spatially unstable mode of the average velocity profile of the wake. The two-dimensional linear analysis on the experimentally measured mean velocity profile in the wake region is performed by Triantafyllou *et al.*[36] They predict that the peak of propulsive efficiency, associated with the optimal jet of strongest momentum for a given input energy, occurs at the frequency corresponding to the maximum spatial growth rate of the mean flow. The optimal range of amplitude-based Strouhal number ($St_A = Af/U_\infty$, where U_∞ is the free stream velocity, f is the oscillation frequency, and A is the scale for the width of the wake and is usually approximated by the peak-to-peak amplitude measured at the trailing edge of the foil) for the

a)Electronic mail: ybao@sjtu.edu.cn

maximum propulsion efficiency was found in the range between 0.25 and 0.35.[35]

Various wake types have been found for a flapping foil depending on St_A. The unstable wake corresponding to thrust production develops in an inverted BvK vortex street, and it occurs in the reversed direction of the vorticity in each vortex[28] with respect to the normal BvK wake observed behind bluff objects.[40] The vortex shedding process in inverted BvK street for a plunging airfoil and normal BvK street behind an oscillating cylinder was presented, respectively, in Lai and Platzer[28] and Williamson and Roshko.[40] Godoy-Diana *et al.*[19] found that wake transition from BvK type to inverted BvK type precedes the actual transition from drag to thrust transition. This means the corresponding St_A for the wake transition is smaller than that for the drag to thrust transition. Moreover, higher St_A triggers symmetry breaking in the wake with the inverted BvK vortex street deflecting from the mean position.[3,20,24,28,29,32,42] Apart from the typical types of BvK and inverted BvK, complex wakes with up to 16 vortices per oscillation period were identified in Schnipper *et al.*[32]

Only a few existing studies have paid attention to the flow interference effect of dual foil configurations. Kaya *et al.*[26] and Tuncer and Kaya[38] numerically investigated the propulsive performance of flapping airfoils in side-by-side configurations. The biplane configuration was observed to improve the thrust force more than 40% when it is compared to the single foil configuration. It is also found that the phase difference between the pitching and heaving motions is critical for the flow development and thrust generation.[38] Kaya *et al.*[26] optimized the flapping kinematics to maximize the thrust production and propulsive efficiency. The highest thrust force was achieved with a Strouhal number between 0.17 and 0.25, however it significantly diminishes with further increased Strouhal number. Miao *et al.*[30] investigated the effect of the chordwise flexure on unsteady aerodynamic characteristics of biplane dual NACA 0014 foils with anti-phase flapping. Their numerical results showed that flexible flapping at appropriate conditions when the flapping airfoil has a flexure extent of 0.25 not only increases the thrust generation but also enhances the propulsive efficiency. Tay *et al.*[34] performed a numerical investigation on the interference of a stationary downstream tail on the propulsion of single or biplane flapping airfoils. They found that by increasing the incidence angle of the tail, the system can achieve a higher lift generation. The impact of tail on the propulsive performance also depends on its location, which is defined as the horizontal distance from the front airfoil and the vertical distance from the wake centerline. Dong and Lu[18] numerically investigated flow over undulating foils arranged in side-by-side configurations with anti-phase and in-phase traveling wavy movements. They demonstrated both the saving of swimming power for the in-phase traveling and the increasing of thrust generation for the anti-phase traveling. Dewey *et al.*[15] revealed that the thrust production and power input are dependent on both the oscillation phase difference and spacing distance for the side-by-side configuration.

While these studies contribute to a better understanding of propulsive characteristics, there is still lack of knowledge on the wake dynamics, which becomes significantly different in the presence of hydrodynamic interference for the flapping system of multi-foils. Open questions include (but are not limited to) the following: (1) How do the inverted BvK streets interact instantaneously with each other and vary with the gap spacing? (2) How do the physical characteristics of the time-averaged wake change with the gap spacing? (3) How do they influence the propulsive performance including both thrust production and power efficiency? The goal of the current investigation is to address these issues for the limited parameter space in which only the pure anti-phase harmonic pitching motions are considered. The geometric configuration of the flapping system is very close to the previous experimental work by Dewey *et al.*,[15] but the current effort highlights the temporal evolution of the wake dynamics and the time-averaged wake properties. As will be shown in this work, the interaction of the two inverted BvK wakes displays various evolution types depending on the gap spacing and the Strouhal numbers.

II. PHYSICAL MODEL AND GOVERNING EQUATIONS

The 2D incompressible Navier-Stokes equations are employed to describe the surrounding flow dynamics of the model system and are written in vector form as follows:

$$\frac{\partial U}{\partial t} + U \cdot \nabla U = -\frac{1}{\rho}\nabla p + \frac{\mu}{\rho}\nabla^2 U, \tag{1}$$

$$\nabla \cdot U = 0, \tag{2}$$

where U is the flow velocity vector with components of (u, v), respectively, in (x, y) Cartesian coordinate directions, p and t are the pressure and time, respectively, and ρ and μ are the density of the fluid and the dynamic viscosity.

The schematic view of the physical model is presented in Fig. 1. Two rigid foils arranged in side-by-side configurations are subject to undisturbed free stream velocity of U_∞. Each foil is outlined by a semicircular leading edge (diameter D) and straight sides (chord length $C = 5.1D$), forming geometric configuration with a sharp trailing edge. The selected geometric lengths lead the foil-width-based Reynolds number, $Re_D(\rho U_\infty D/\mu)$, to be 250, which corresponds to the chord-based Reynolds number $Re_C(\rho U_\infty C/\mu) = 1275$, characterizing flapping-based propulsion in nature. This is slightly larger than that used in the experimental studies reported in Godoy-Diana *et al.*[19] The motions of

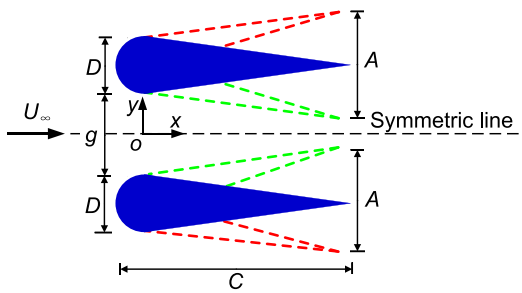

FIG. 1. Schematic diagram of an anti-phase flapping system consisted of two rigid foils arranged in side-by-side configuration.

two foils are prescribed as counter-phase regime harmonic pitching oscillations. The parameter ratio g/D is used to describe the relative locations of the two foils, where g denotes the face-to-face transverse distance of the leading edge.

The kinematics of the flapping bodies are described by a harmonic pitching motion with dimensionless oscillation amplitude $A_D = A/D$ and foil width-based Strouhal number $St_D = Df/U_\infty$ (A and f are, respectively, of flapping amplitude and frequency), which are given as

$$Y_u(t) = 0.5A_D \sin(2\pi St_D t),\ Y_l(t) = 0.5A_D \sin(2\pi St_D t + \pi), \tag{3}$$

where $Y_u(t)$ and $Y_l(t)$ are the time-dependent transverse displacements of the trailing edge for the upper and lower foils, respectively.

A wide range of kinematic parameter space (A_D, St_D) is investigated, varying in the range of $0.4 \le A_D \le 2.0$ and $0.15 \le St_D \le 0.45$, which corresponds to the wake-width-based Strouhal number ranging in $0.06 \le St_A \le 0.55$. The simulation is restricted in closely arranged configurations, with the gap spacing g/D ranging from 1.0 to 4.0.

III. NUMERICAL METHODS

The momentum equation is reformulated in the Arbitrary-Lagrangian-Eulerian (ALE) form to take into account of the effect of moving boundaries. A field variable of velocity vector, $\hat{U} = (\hat{u}, \hat{v})$, is introduced to modify the convective term in Equation (1) such that $(U - \hat{U}) \cdot \nabla U$ for describing the flow convection in the ALE reference framework, as proposed originally in Donea *et al.*[17] and Hughes *et al.*[23] ($\hat{u}$, $\hat{v}$), are the velocity components of the moving computational domain in (x, y) directions. In the ALE reference, the kinematics of the material point on moving boundaries is stated by Lagrangian description, while an Eulerian description can be used at a certain distance from moving surfaces, as well as all the remaining boundaries. In practice, a modified spring-analogy algorithm is employed in this work to update $\hat{U}$ and the mesh system associated with it.[41]

TABLE I. Convergence test for an isolated pitching foil at $St_A = 0.45$.

Case number	Number of elements	Number of nodes	Mesh size on the wall	$\bar{C}_T$
#1	86 050	45 701	0.01D	1.721
#2	107 220	55 335	0.006D	1.886
#3	137 652	68 117	0.004D	1.902

The fractional step method in the framework of Characteristic-Based-Split (CBS) scheme is used to decouple the calculation of the velocity and pressure fields. An elliptic pressure-Poisson equation is derived from the discretized momentum equations and the continuity equation. A stabilized pressure gradient projection method[12,13] is employed to eliminate the artificial oscillation that would occur in pressure field. The three-node linear triangular element is used to approximate the interpolation functions of both the velocity and pressure over the solution space. The details can be referred to Bao *et al.*[8] and Han *et al.*[22] The kinetic motion of the pitching foil is described from the prescribed sinusoidal function that was given in Equation (3).

The governing equations of the flow model are solved with the appropriate boundary conditions: a uniform velocity profile is imposed on the inlet boundary, which is specified as $u = U_\infty$ and $v = 0$; Neumann boundary conditions of $\partial u/\partial x = 0.0$ and $\partial v/\partial x = 0.0$ are applied on the far downstream outlet; the lateral boundaries are treated to be slip boundaries, i.e., $\partial u/\partial y = 0.0$ and $v = 0.0$; a no-slip boundary condition is prescribed at the surface of the two foils such that $u = \hat{u}$ and $v = \hat{v}$.

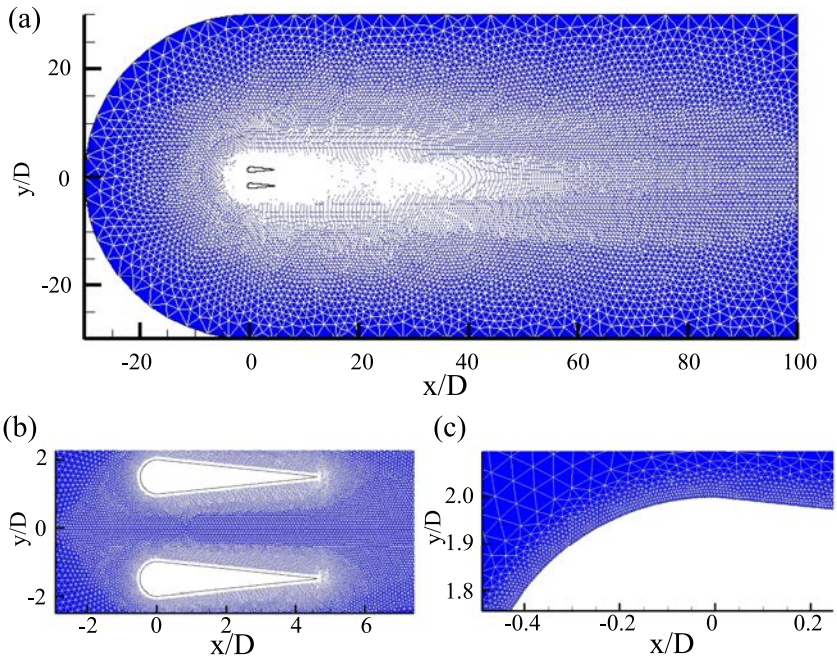

FIG. 2. Computational mesh used for the simulations at $g/D = 2.0$: (a) view of the entire domain; (b) closed view of the side-by-side model; and (c) closed view of a part of the leading edge.

The computational domain of the current simulation is given such that the outflow boundary is located 100D far away from the origin O of the coordinate system, while the upstream boundary is profiled in semi-circular with the radius of 30D and the lateral boundaries are located 30D away from the symmetric line of the wake. The convergence test was conducted (see Table I) and the mesh resolution of this study is similar to our previously published work;[4] the entire mesh contains 107 220 elements and 55 335 nodes and a grid size of 0.006D along the foil surfaces is accurate enough for our simulations. The grid in the wake region is refined suitably for capturing the dynamic detail of the wake evolution. The sketch of the computational domain with mesh discretization and its closed view of the flapping model is given in Fig. 2. The non-dimensional time step size used in the simulation is fixed to be 0.002.

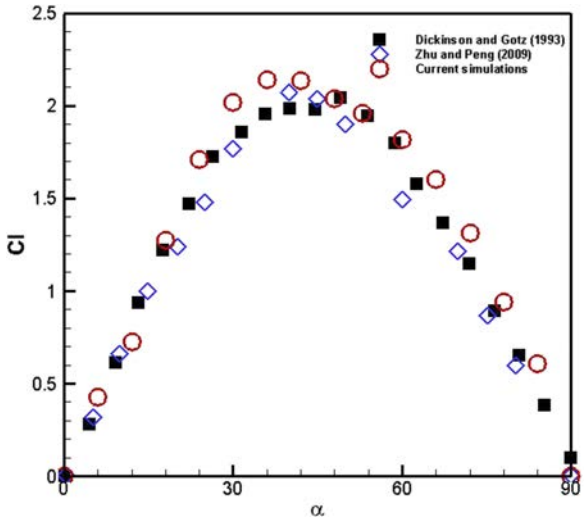

FIG. 3. Comparison of the lifting coefficient on a fixed thin foil.

IV. VALIDATION OF THE NAVIER-STOKES EQUATION SOLVER

The in-house code has been validated widely for the case of vortex-induced vibration of elastically mounted circular cylinders.[5–7,37] In this work, further validation is presented and a benchmark case is considered where the foil has a fixed angle of attack (α) and compares the lift force against both the experimental and numerical data reported in the literature.[16,44] The selected thin foil has the same geometric profile used in Zhu and Peng[44] and the Reynolds number based upon the chord length also has the same value (Re_C = 192). As plotted in Fig. 3, the comparison of the lift force exhibits good agreement with both the experimental measurement[16] and numerical predictions.[44]

In the second case, the wake patterns behind an isolated pitching foil is examined to compare against the experimental study[32] under the same conditions of A_D and St_D. As reported in Schnipper *et al.*,[32] the chord-based Reynolds number of two different values (Re_C = 1320 and 2640) was considered in the experimental work depending on St_D. Schnipper *et al.*[32] also stated that the wake structures and transitions are insensitive to the values of Reynolds number provided the foils are not subject to three-dimensional instabilities. By varying the frequency and amplitude of the oscillation of a symmetric foil undergoing pitching oscillations in a vertically flowing soap film, Schnipper *et al.*[32] identified a variety of pattern type of vortex shedding, including 2S BvK street, 2S inverted BvK street, 2P wake, 2P + 2S wake, 4P + 2S wake, 6P + 2S wake, and 8P wake as well.

The vorticity contours from the current computations of wake fields, which are under the same conditions of A_D and St_D used in Schnipper *et al.*,[32] are presented in Fig. 4. A classic 2S BvK street can be identified for the parameter combinations of (A_D, St_D) = (0.88, 0.12) and (0.98, 0.12), as observed in Figs. 4(a) and 4(b). Two types of 2P and 2P + 2S are presented in (A_D, St_D) = (1.4, 0.08) and (1.2, 0.053), respectively (see Figs. 4(e) and 4(d)). The wakes for (A_D, St_D) = (1.2, 0.035), (1.34, 0.039), and (1.47, 0.035) display similar types

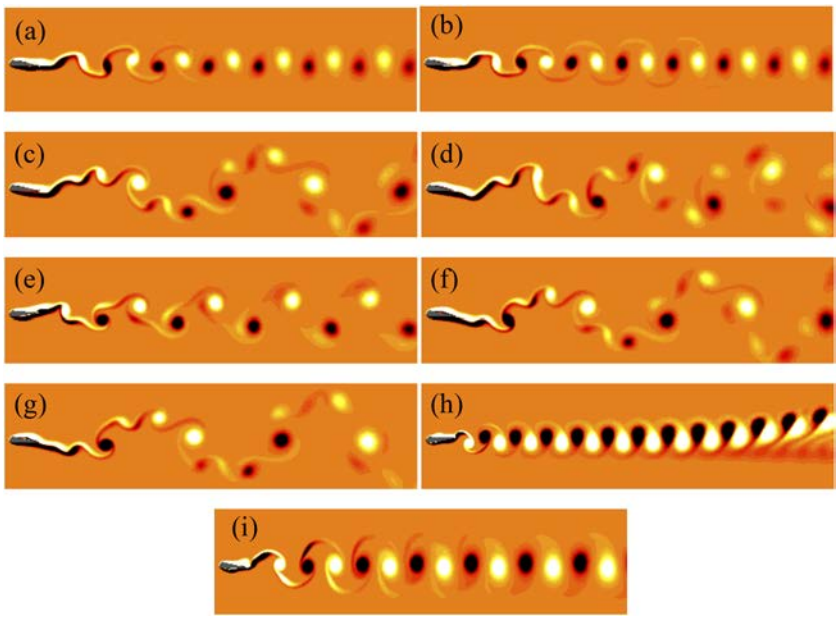

FIG. 4. Wake patterns behind an isolated foil for different parameter combinations: (a) (A_D, St_D) = (0.88, 0.12); (b) (A_D, St_D) = (0.98, 0.12); (c) (A_D, St_D) = (1.2, 0.035); (d) (A_D, St_D) = (1.2, 0.053); (e) (A_D, St_D) = (1.4, 0.08); (f) (A_D, St_D) = (1.34, 0.039); (g) (A_D, St_D) = (1.47, 0.035); (h) (A_D, St_D) = (1.335, 0.25); (i) (A_D, St_D) = (2.0, 0.12).

and can be sorted out into a type of 4P (see Figs. 4(c), 4(f), and 4(g)). In a phase diagram spanned by the Strouhal number and the amplitude, Schnipper *et al.*[32] identified a type, called as 4P + 2S, which is very close to 4P with additional 2S per oscillation cycle. Since the 2S vortices in 4P + 2S are too weak, it is hard to identify them in the current simulations. Finally, the 2S inverted BvK street is identified in the wake of $(A_D, St_D) = (1.335, 0.25)$ and (2.0, 0.12) (see Figs. 4(h) and 4(i)). The observation thus shows that most of the wake patterns reported in Figure 3 in Schnipper *et al.*[32] were predicted numerically, reaching a good agreement between the experimental and numerical studies.

V. NUMERICAL RESULTS OF ANTI-PHASE FLAPPING SYSTEM

A. Propulsive performance

The propulsive performance of the two-foil flapping model in the sense of time average is investigated in Fig. 5, where the mean values of the thrust force coefficient, $\bar{C}_T$, power coefficient, $\bar{C}_P$, and propulsive efficiency, η, are given as functions of St_A for various gap spacings. Since upper and lower foils experience approximately equal thrust force, only the results of the upper foil are plotted in this figure. The time-dependent thrust coefficient, $C_T(t)$, and power coefficient, $C_P(t)$, are defined here as $C_T(t) = -2F_D(t)/\rho U_\infty^2 D$ ($F_D(t)$ is the hydrodynamic force component in horizontal direction and is obtained from the integration of both pressure and viscous parts around the surface of the foil) and $C_P = 2P(t)/\rho U_\infty^3 D$ ($P(t) = M(t)d\theta(t)/dt$ is the input power required for pitching the foil, where $M(t)$ is the moment at the pitching axis and $\theta(t)$ is associated pitching angle), respectively.

It can be observed that in the drag generation regime ($\bar{C}_T < 0.0$, see in Fig. 5(a)), the flapping foils exhibit similar hydrodynamic properties for different gap distances. This observation is confirmed by the near collapse of the variation curves with the isolated flapping foil case. The interaction effect of the two foils becomes significant only in the thrust generation regime ($\bar{C}_T > 0.0$). A higher thrust is generally produced from closer proximity arrangement of the system for a fixed Strouhal number. On the other hand, the transition from drag to thrust occurs at lower Strouhal number for smaller gap spacing, implying an earlier wake transition from the normal BvK to inverted BvK-type as the gap distance decreases.

It can be observed from Fig. 5(b) that the power coefficient also increases with the increasing St_A. On the other hand, for a fixed St_A, a smaller gap spacing always leads to a higher power consumption, especially for the higher St_A. This observation indicates that a competitive mechanism between the thrust production and the power consumption involves and that eventually determines the propulsive efficiency of the flapping foil system.

The propulsive efficiency is defined as the ratio of useful power to input power, i.e., $\eta = U_\infty \bar{C}_T/\bar{C}_P$, which is plotted against St_A in Fig. 5(c). At $g/D = 1.0$, the efficiency is maximized at $St_A = 0.28$ with a value of $\eta = 0.223$. This is approximately 37.6% higher than the maximum value of an isolated foil at $St_A = 0.55$ ($\eta = 0.162$). As the gap increases to $g/D = 4.0$, the Strouhal frequency associated with the highest efficiency shifts to a higher Strouhal frequency of $St_A = 0.45$. The calculated maximum efficiency ($\eta = 0.221$) is slightly smaller than the case of $g/D = 1.0$. The performance at different gap spacing then shows that the optimal St_A for the peak efficiency shifts to a lower value with the decreasing gap distance. It is noted that the calculated

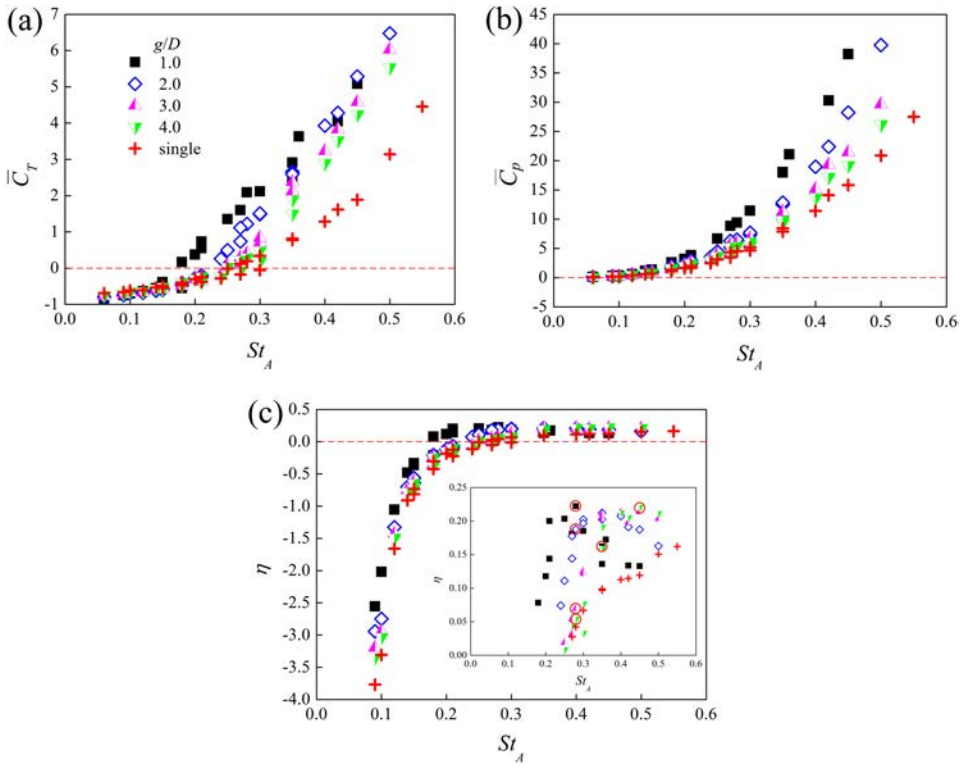

FIG. 5. Propulsive performance of the two-foil flapping system: (a) thrust coefficient; (b) power coefficient; and (c) propulsive efficiency as a function of the Strouhal number.

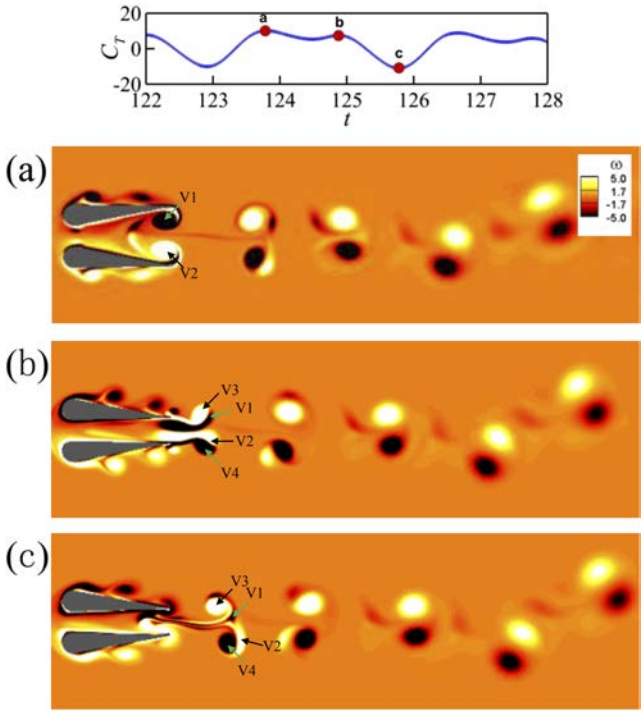

FIG. 6. The wake at $(A_D, St_A, g/D) = (1.0, 0.35, 1.0)$: instantaneous successive vorticity contours associated with the phase points marked by a, b, and c in the time history of C_T. The negative vorticity in black color rotates in the clockwise direction and the positive vorticity in white color rotates in the counter-clockwise direction.

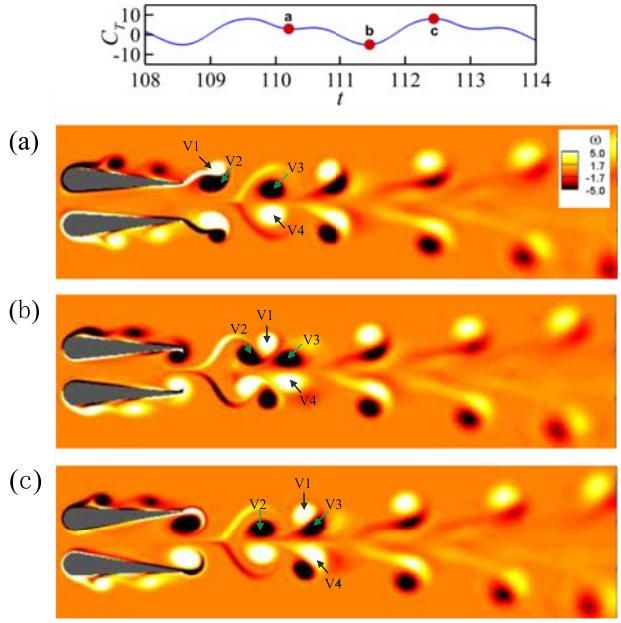

FIG. 7. The wake at $(A_D, St_A, g/D) = (0.8, 0.28, 1.0)$: instantaneous successive vorticity contours associated with the phase points marked by a, b, and c in the time history of C_T. The negative vorticity in black color rotates in the clockwise direction and the positive vorticity in white color rotates in the counter-clockwise direction.

optimal St_A for the isolated foil was found to be somewhat higher than the previously published data for heaving and pitching foils.[35,36] Recently, Deng *et al.*[14] conducted a numerical study on the correlation between wake transition and propulsive efficiency of a foil with the motion of both pitching and heaving. Their numerical results of pure pitching foil show that the trend of propulsive efficiency against St_A is dependent on Re_C. The value of St_A associated with the maximum η increases with the decrease of Re_C. At $Re_C = 1000$, which is close to the case in this study, the maximum η is achieved at $St_A = 0.7$. Noted that in this study, the examined St_A is limited to 0.55 for the isolated foil, but it shows a consistent trend with the results from Deng *et al.*[14] In summary, the propulsive performance is significantly affected by the gap spacing and the optimal Strouhal number associated with the highest efficiency is increased with the increase of the gap spacing. In Secs. V B and C, some representative cases (marked in red circles in Fig. 5(c)) are selected to investigate both their transient and time-averaged wake properties.

B. Instantaneous wake dynamics

As observed in Sec. V A, the propulsive performance displays different hydrodynamic characteristics, depending on the gap spacing. In order to explore what gives rise to such difference, in Secs. V B and V C, the wake features of the anti-phase flapping system are investigated. Few representative cases as marked by red circles in Fig. 5(c) are chosen to present how the transient and time-averaged wake dynamics change with the propulsive properties.

Figs. 6 and 7 exhibit the instantaneous wake flows for the two cases with the parameter combinations of $(A_D, St_A, g/D) = (1.0, 0.35, 1.0)$, and $(0.8, 0.28, 1.0)$. Each case provides three successive snapshots of the vorticity contours in a full flapping cycle. As demonstrated in the following, the wake features of these cases are characterized mainly by the mechanism of vortex reorganization that involves in the whole wake evolution process.

A strong wake interference from the upper and lower sides can be exhibited at the flapping amplitude of $A_D = 1.0$, as demonstrated in the wake evolution shown in Figs. 6(a)–6(c). In the convection process, two inverted BvK streets are unified into an unitary one. Specifically, the vortices formed on the inner side of the foils (marked by $V1$ and $V2$) are dissipated in the gap area; on the other hand, the vortices formed on the free stream sides (marked by $V3$ and $V4$), are shed, respectively, from the free stream side of each foil and eventually organized in a vortex pair of momentum jet. The downwash velocity that is induced by this counter rotating

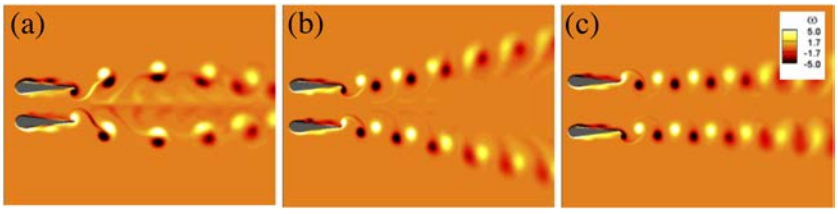

FIG. 8. Comparison of instantaneous vorticity contours at $(A_D, St_A) = (0.8, 0.28)$ with different gap spacing: (a) $g/D = 2.0$; (b) $g/D = 3.0$; and (c) $g/D = 4.0$. The negative vorticity in black color rotates in the clockwise direction and the positive vorticity in white color rotates in the counter-clockwise direction.

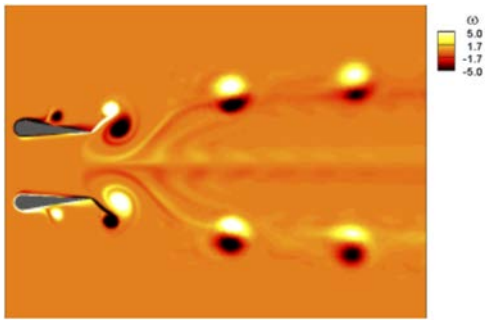

FIG. 9. Instantaneous vorticity contours at (A_D, St_A, g/D) = (1.8, 0.45, 4.0). The negative vorticity in black color rotates in the clockwise direction and the positive vorticity in white color rotates in the counter-clockwise direction.

vortex pair conforms to the characters of momentum jet in the wake. This can also be confirmed by the time-averaged velocity profile as will be shown in Fig. 13(a). In addition, the wake symmetry is apparently broken due to the strong wake flow mixing from the two sides. As we recall the hydrodynamics of this case, a significant thrust force is generated from this single momentum jet; however, the annihilation of vortices in the gap side may exhaust an amount of energy, explaining the decrease of the propulsive efficiency relative to the maximum one (see the marked square point in Fig. 5(c)).

Wake interference at further higher Strouhal number ($St_A > 0.4$) would make the wake evolution to become chaotic (not shown here) and that is responsible for the significant deterioration of propulsive efficiency in Fig. 5(c).

As discussed in Subsection V A, the propulsive efficiency is maximized at (A_D, St_A) = (0.8, 0.28) for the fixed gap spacing of g/D = 1.0. The power consumption of this case ($\bar{C}_P$ = 9.40) is quite lower as compared to the case at the point of (A_D, St_A) = (1.0, 0.35), where the power coefficient reaches a value as large as $\bar{C}_P$ = 17.96, which is nearly two times of the former case; however, the thrust generation of the two cases likely maintains at the same level. The thrust coefficients are $\bar{C}_T$ = 2.09 at the point (A_D, St_A) = (0.8, 0.28) and $\bar{C}_T$ = 2.91 at the point (A_D, St_A) = (1.0, 0.35). In order to reveal the associated flow dynamics for the propulsive performances, the wake evolution is then detected in Fig. 7. As shown in Figs. 7(a)–7(c), a symmetric evolution with respect to the centerline is observed. The flow evolves to form a different wake configuration as compared to the previous case. The primary feature is that the inverted BvK streets coexist in parallel form but the wake interaction reorganizes the vortex distributions along the streets too. In a more specific way, in Fig. 7(a), the anti-phase flapping foils produce a fully developed vortex pair behind the trailing edge of each foil, which consists of anti-rotating vortices (marked in the plot by $V1$ and $V2$). In the following image shown in Fig. 7(b), a downstream vortex pair ($V3$ and $V4$ arranged in wake-like manner) dynamically changes the convective trajectory of the upstream pairs, causing vortex condensation along the wake centerline. The interaction process further induces vortex rearrangement as observed in Fig. 7(c), in which two pairs of vortex (for instance, the upper pair consists of $V1$ and $V3$) are organized in jet-like manner and the third one is organized in wake-like manner, in which one vortex (i.e., $V2$) is shed from the upper side and the other is from the lower side. In the observed wake evolution, the formation of the gap vortices does not consume energy as much as that in the previous case, which is beneficial for the improvement of the propulsive performance and will be further demonstrated in the time-averaged velocity profile discussed in Sec. V C.

For the fixed point of (A_D, St_A) = (0.8, 0.28), as observed in Fig. 5, the thrust production and efficiency decrease significantly with the increasing gap. Correspondingly, the associated vorticity contours are plotted in Fig. 8 at varying gap spacing in the range of g/D = 2.0–4.0. The formation of an inverted BvK street behind each foil is observed and it develops separately in symmetric configuration at the two sides of the mean position (or symmetric line of the wake, see Fig. 1). However, the convective trajectory of the vortex pairs in the near wake region is different, which is depending on the gap spacing. At g/D = 2.0, they are deflected away from each other and evolved in inward curved shape in the near wake region (see Fig. 8(a)). For the cases where the gap spacing is larger, the wake interference becomes weaker as evidenced in the shedding features shown in Figs. 8(b) and 8(c). The formation of inverted BvK street looks similar to that observed behind an isolated flapping foil. Wake deflection is noticed in the case of g/D = 3.0, but it will finally become parallel in relevant to the wake centerline (not shown here). When the gap is increased to g/D = 4.0, the inverted BvK streets become totally parallel in the wake. As a consequence, the propulsive performance including both the thrust force and power consumption is close to that of an isolated foil (see Fig. 5). It is interesting that the wake path motion is different with the variation of the gap spacing. It can be explained by the convective velocity of the

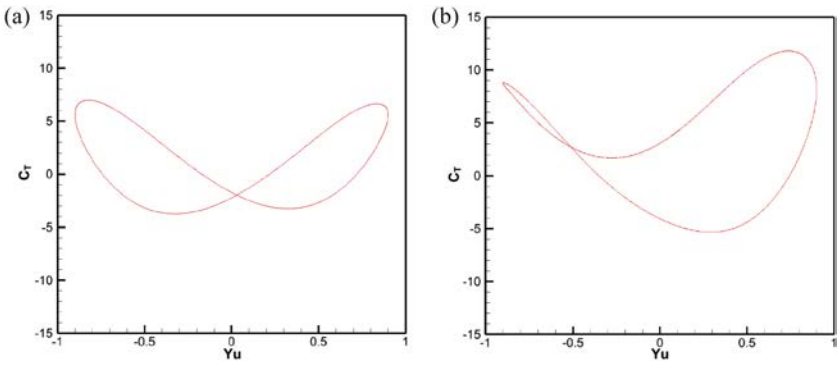

FIG. 10. Comparison of the phase portrait of the thrust coefficient relative to the transverse displacement of the trailing edge against the case of an isolated foil: (a) (A_D, St_A) = (1.8, 0.45), an isolated pitching foil and (b) (A_D, St_A, g/D) = (1.8, 0.45, 4.0).

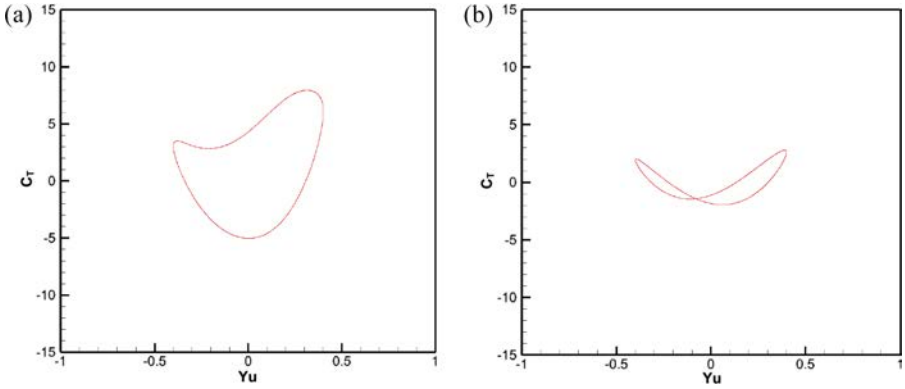

FIG. 11. Comparison of the phase portrait of the thrust coefficient relative to the transverse displacement of the trailing edge at different gap spacing with $(A_D, St_A) = (0.8, 0.28)$: (a) $g/D = 1.0$ and (b) $g/D = 3.0$.

vortex pairs along the inverted BvK street. For the case at $g/D = 2.0$, the convective velocity of the vortex at the gap side is remarkably smaller than that of the vortex at the free stream side. This can also be demonstrated by the significant deficit of velocity profile at the gap side of the jet peaks as will be shown in Fig. 16(a). As a result, the path motion of the vortex pair curves inward due to the dynamic interactions of each other. In contrast, the repelling motion at gap spacing of $g/D = 1.0 (x/D > 13.6)$ and $g/D = 3.0$ is relevant to the recovered velocity at the gap side of the jets. Wake deflection for an isolated flapping foil is frequently reported in the literature.[19,20,43] As compared to an isolated flapping foil, the deflection occurs at relatively lower St_A in the two-foil flapping system. While the deflection observed here is induced from the effect of wake interference, the symmetry breaking of an isolated foil is probably related to the triggering of the onset of asymmetric mode in wake instability mechanism. A phenomenon of symmetry breaking is also observed in the wake of an oscillating cylinder as reported in Blackburn and Ron[9] and Griffin and Ramberg.[21] However, the issue on the symmetric breaking and related wake instability of an oscillating body is still open to discussion. For the larger gap spacing of $g/D = 4.0$, increasing Strouhal frequency intensifies the wake interaction. This is evident in the evolution of inverted BvK streets in a curved shape at the larger Strouhal number of $St_A = 0.45$ (see Fig. 9).

The phase portraits of the thrust coefficient (C_T) with respect to the time-dependent transverse displacement (Y_u) of the trailing edge are plotted in Figs. 10 and 11. In Fig. 10 the case of the upper foil at $g/D = 4.0$ is compared with the case of isolated foil for the same pitching parameters of $(A_D, St_A) = (1.8, 0.45)$. A symmetric portrait in the shape of "∞" as shown in Fig. 10(a) indicates that the thrust force of an isolated foil oscillates at a frequency twice of that of pitching oscillation. The symmetry of the portrait is typically broken due to the effect of the wake interference for the two flapping foil system (see Fig. 10(b)). The effect of the gap spacing on the phase portrait can be revealed in Fig. 11. The phase portrait follows a deformed circle at a smaller gap of $g/D = 1.0$, which is consistent with the deformed wake of reorganized vortices in the inverted BvK streets. On the other hand, the case at larger gap is comparable to the case of an isolated foil even though the Strouhal number is different. From these observations a monotonic approach of the wake dynamics of the foil-foil system to the case of an isolated foil may be expected when the gap increasingly rises.

As described before, the drag-thrust transition occurs earlier in terms of Strouhal frequency for smaller gap spacing. Fig. 12 presents the transient wake features for different cases where the thrust (or drag) coefficients are close to zero at $g/D = 1.0$. In the specific cases, the drag is generated at $(A_D, St_A) = (0.6, 0.15)(\bar{C}_T = -0.387)$, $(A_D, St_A) = (1.0, 0.15)(\bar{C}_T = -0.494)$, and $(A_D, St_A) = (1.2, 0.18)(\bar{C}_T = -0.551)$, while the thrust is produced at $(A_D, St_A) = (0.4, 0.18)(\bar{C}_T = 0.165)$, $(A_D, St_A) = (0.6, 0.21)(\bar{C}_T = 0.549)$, and $(A_D, St_A) = (0.8, 0.20)(\bar{C}_T = 0.374)$. It can be observed that the wake shedding associated with the drag production is characterized by a wake-like counter rotating vortex pair (marked by a circle in Fig. 12(e), where the arrow indicates the velocity direction induced by this vortex pair) that is formed in mushroom shape. In contrast, the wake interaction becomes more energetic when the thrust generation is involved. This is evidenced by the formation of jet-like vortex pair (marked by a circle in

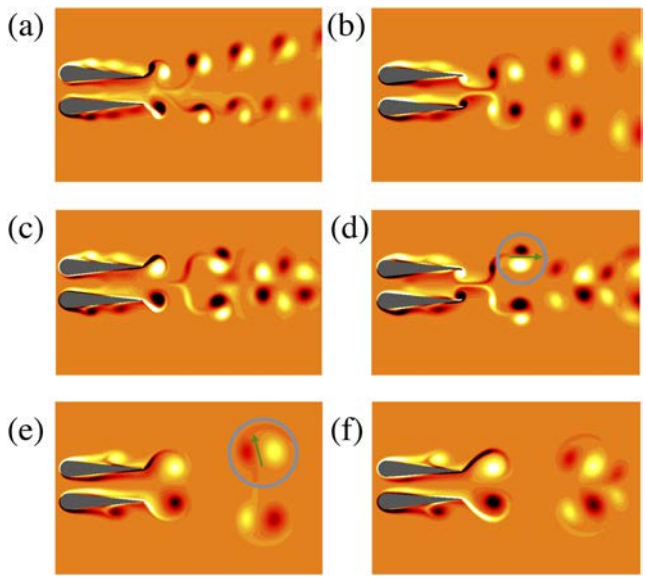

FIG. 12. Instantaneous vorticity contours at $g/D = 1.0$: (a) $(A_D, St_A = 0.4, 0.18)$; (b) $(A_D, St_A = 0.6, 0.15)$; (c) $(A_D, St_A = 0.6, 0.21)$; (d) $(A_D, St_A = 0.8, 0.20)$; (e) $(A_D, St_A = 1.0, 0.15)$; and (f) $(A_D, St_A = 1.2, 0.18)$. The negative vorticity in white color rotates in the clockwise direction and the positive vorticity in black color rotates in the counter-clockwise direction.

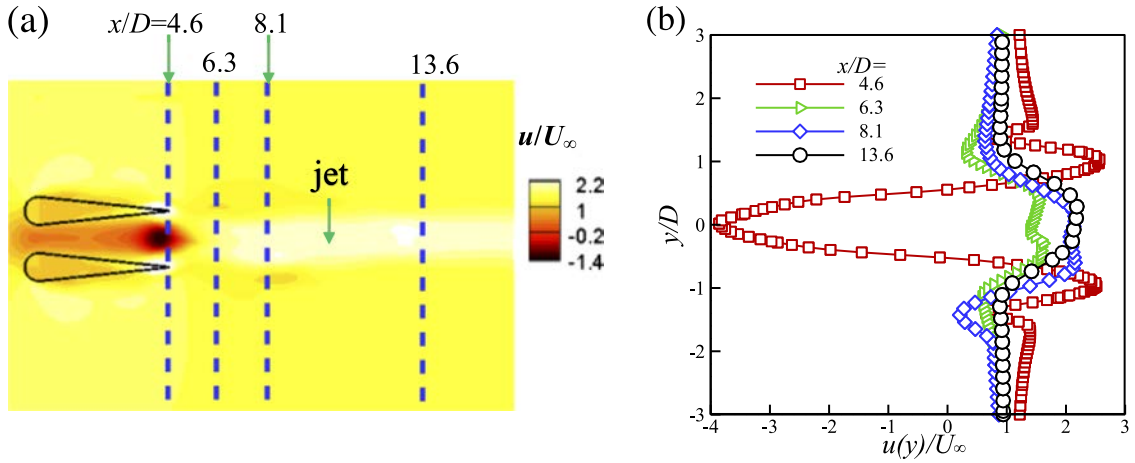

FIG. 13. Time-averaged wake characteristics at (A_D, St_A, g/D = 1.0, 0.35, 1.0): (a) streamwise velocity contour and (b) streamwise velocity profiles.

Fig. 12(d)) due to the intensified wake interactions. It is interesting that an asymmetric wake is noticed at (A_D, St_A) = (0.4, 0.18). In particular, the inverted BvK street generated from the upper foil is deflected away from the symmetric line; on the other hand, the street behind the lower foil is parallel to the symmetric line. The physical mechanism for this observation is beyond the scope of this work. Interestingly, it can also be observed that although the amplitude-based Strouhal frequency is the same, totally different force generation is evidenced for the two cases of (A_D, St_A) = (1.2, 0.18) and (0.4, 0.18). This observation indicates that flapping frequency characterized by

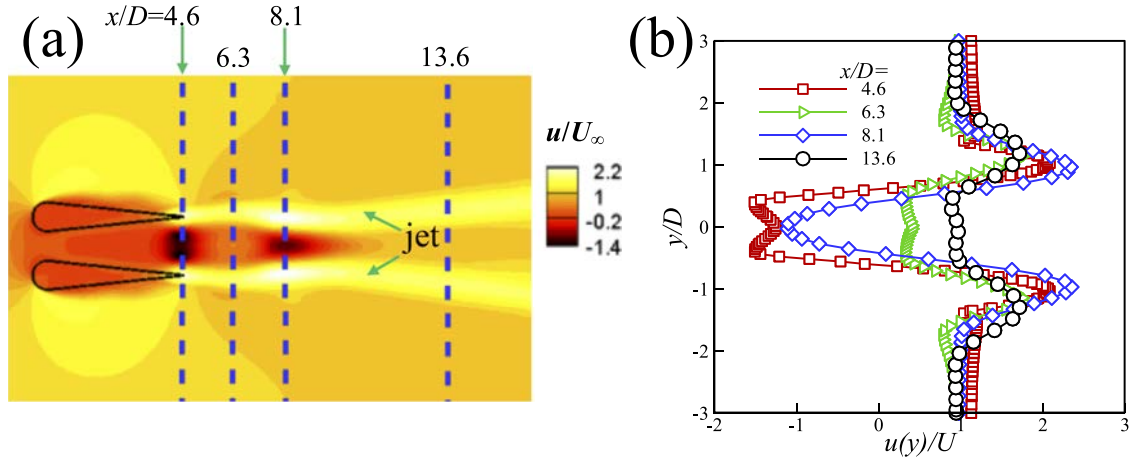

FIG. 14. Time-averaged wake characteristics at (A_D, St_A, g/D = 0.8, 0.28, 1.0): (a) streamwise velocity contour and (b) streamwise velocity profiles.

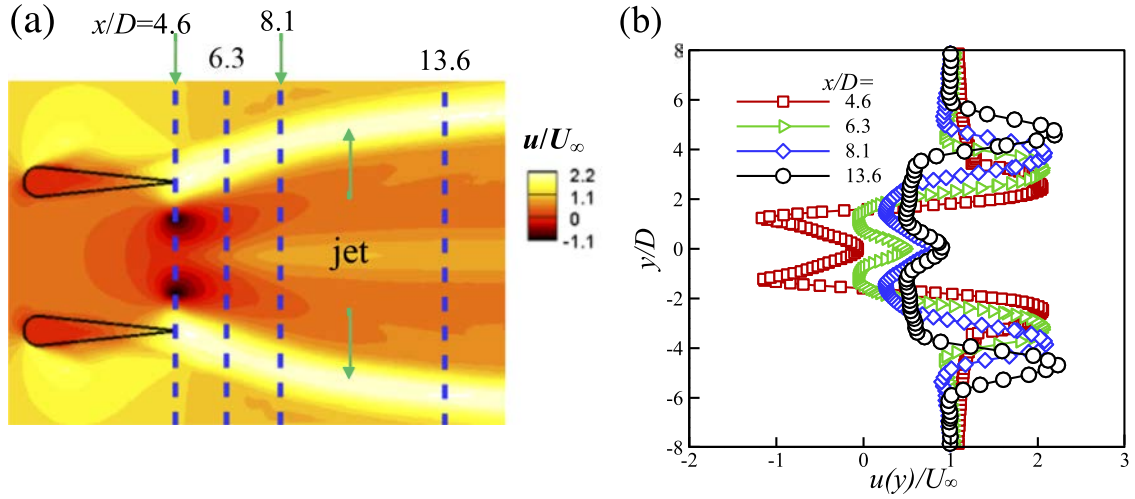

FIG. 15. Time-averaged wake characteristics at (A_D, St_A, g/D) = (1.8, 0.45, 4.0): (a) streamwise velocity contour and (b) streamwise velocity profiles.

the diameter-based Strouhal frequency is significant for the propulsive properties of foil-foil system.

The flow interference of bluff bodies in side-by-side configuration has been widely investigated previously.[1,10,11,25,27,31] The flow regimes corresponding to the wake interactions of such bluff bodies are commonly categorized into anti-phase synchronization, in-phase synchronization, flip-flopping, quasi-periodic, and chaotic as well.[11,25,27] The flows observed behind the flapping foils show similar physical features to that for side-by-side placed bluff-bodies. For instance, anti-phase synchronization exists widely for the inverted BvK streets behind the anti-phase pitching foils. Dewey *et al.*,[15] Dong and Lu[18] and Tuncer and Kaya[38] also revealed in-phase synchronization in the wake of an in-phase flapping foils. However, the current study implicates that the wake interactions become more

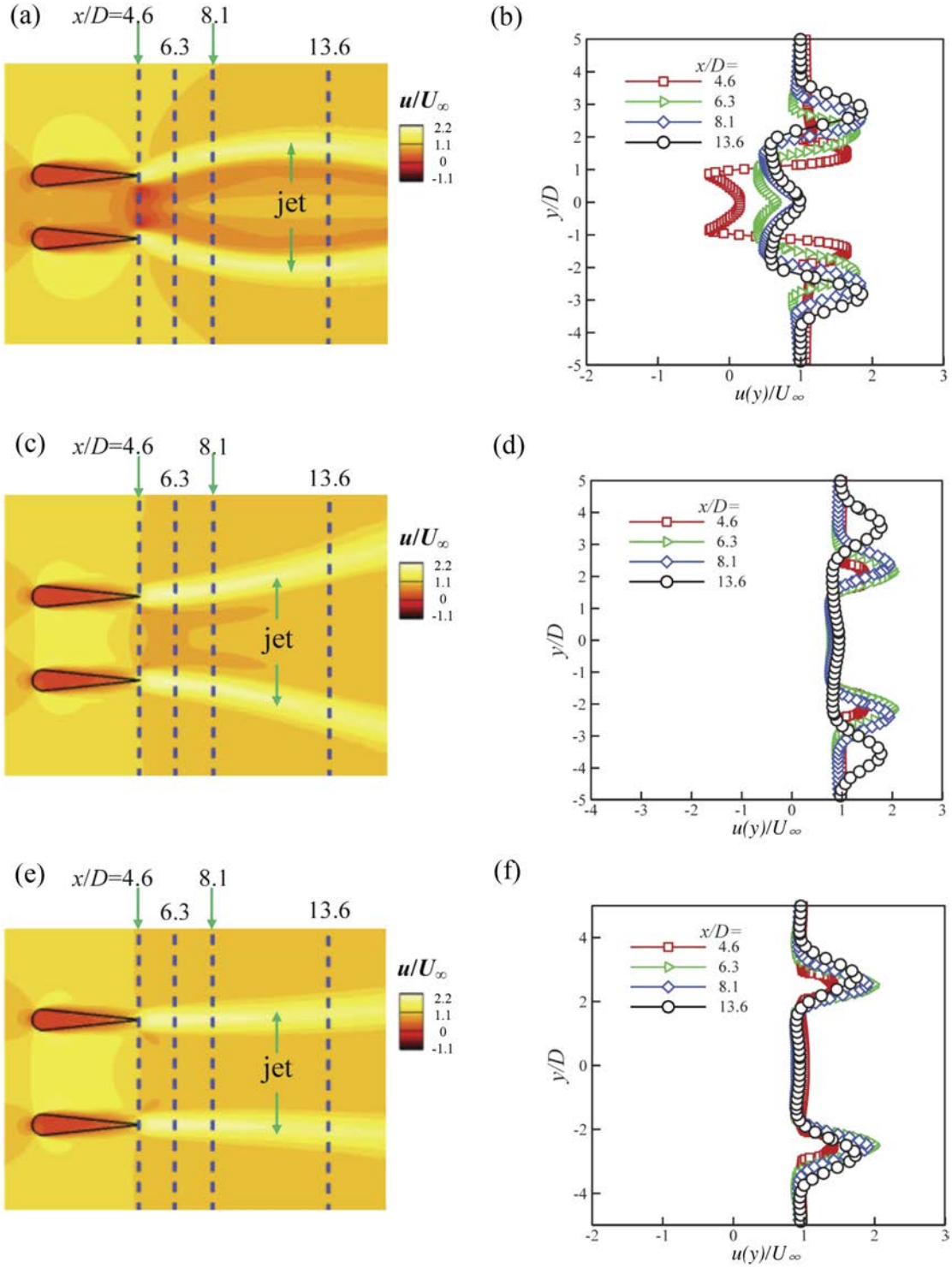

FIG. 16. Time-averaged wake characteristics at different gap spacing with $(A_D, St_A) = (0.8, 0.28)$: (a) streamwise velocity contour and (b) streamwise velocity profiles at $g/D = 2.0$; (c) streamwise velocity contour and (d) streamwise velocity profiles at $g/D = 3.0$; (e) streamwise velocity contour and (f) streamwise velocity profiles at $g/D = 4.0$.

energetic and active in contrast to the wake interference of bluff bodies. This is confirmed by the jet-mixing and vortex re-organization mechanisms revealed in this study.

C. Time-averaged wake dynamics

In this section, the time-averaged wake features are further investigated by examining the streamwise velocity profiles at different wake locations and the streamwise velocity contours as well. The time-averaged wake of the case with (A_D, St_A, g/D) = (1.0, 0.35, 1.0) observed in Fig. 13 also shows coherent characteristics with respect to the instantaneous wake presented in Fig. 6. As shown in Fig. 13, a strong wake deficit ($u/U_\infty \approx -4.0$, $y = 0$) is formed in the gap region at $x/D = 4.6$, which is associated with the formation of vortices in the gap side (see Fig. 6(a)). However, the streamwise velocity quickly changes to a jet profile when $x/D > 6.3$.

As described earlier, in the second case of (A_D, St_A, g/D) = (0.8, 0.28, 1.0), where maximum power efficiency is achieved, the mean wake also confirmed a strong interference that is also observed in the transient wake flow. Correspondingly, in the time-averaged flow shown in Fig. 14, it is noticed that the wake interference causes second deficit peak, which is located around the position of $x/D = 8.1$. This peak is closely correlated with the formation of vortex pair (see V3 and V4 in Fig. 7(a)) in the vortex condensation process. In the far downstream, the two jets are separated and the velocity deficit is fully recovered (see Fig. 14(b)).

The associated time-averaged properties of transient flow shown in Fig. 9 are plotted in Fig. 15. The mean field of streamwise velocity is characterized by two jets that are curved symmetrically at the two sides of the wake for both cases. In the downstream region of the gap, the velocity deficit is not fully recovered even at the far downstream location of x/D = 13.6. The local peak observed at the mean position is also associated with the wake interference between the two foils. By examining again the instantaneous wake shown in Fig. 9, it can be noticed that the stretching of the vortex tail that is produced at the free stream side subsequently splits away from the major structure. Finally, a symmetric structure is formed along the wake centerline, which hence induces downstream velocity peak locally.

The influence of the gap spacing can be illustrated in Fig. 16, where the gap spacing is varied from $g/D = 2.0$ to 4.0 at (A_D, St_A) = (0.8, 0.28). The wake at $g/D = 2.0$ presents similar profiles with the previous case at (A_D, St_A, g/D) = (1.8, 0.45, 4.0), sharing both the curved jets and local peaks at the mean position of the wake. As the gap increases to $g/D = 3.0$, the path of the jets are drifted away from each other. This looks consistent with the interaction type of inverted BvK streets shown in Fig. 8(b). The wake interference at these pitching parameters can nearly be neglected for $g/D = 4.0$, and the velocity profile downstream of the gap is almost unchanged from that at the free stream side.

VI. CONCLUDING REMARKS

Dynamic wake interference of two-foil pitching system in side-by-side arrangement with varying gap spacing in a two-dimensional flow regime is investigated in this work. Two-dimensional Navier-Stokes equations are solved to study the flow dynamics and the two foils are subjected to a harmonic pure anti-phase pitching motion with prescribed oscillation amplitude and frequency. The numerical results show that the dynamic interference has significant influence on the propulsive properties as well as the wake features characterized in formation and evolution of inverted BvK streets. Some main findings are summarized as follows:

For a fixed gap spacing, the foil-foil system shows similar trend of propulsive properties against varying Strouhal number; however, the optimal Strouhal frequency associated with the maximum efficiency shifts to a smaller value with the decreased gap spacing. The propulsive efficiency is maximized at (St_A, g/D) = (0.28, 1.0) with a value of $\eta = 0.223$, which is approximately 37.6% higher than the maximum value of an isolated foil at $St_A = 0.55$ ($\eta = 0.162$). Also, the drag to thrust transition occurs earlier at smaller Strouhal number as the gap spacing decreases.

For the case of strong wake interference typically at g/D = 1.0, the evolution of wake involves the mechanism of vortex reorganization in the inverted BvK street. Specifically, the wake associated with the higher efficiency is typically reorganized into either a unitary jet-like flow in a single inverted BvK street or highly interacting two inverted parallel BvK streets. Chaotic wake at further increased Strouhal number remarkably deteriorates the propulsive efficiency. Wake interference at larger gap spacing generally induces the deflection of inverted BvK street in a curved shape, and the propulsive performance for this situation is dominated by the pitching parameters.

The time-averaged velocity profiles reveal that the strong wake interference at closer gap spacing is accompanied by distinct velocity deficit in the gap area, which may be the result due to the generation process of vortex pair at the gap side of trailing edge or the wake interaction in the downstream wake. For the case where the maximum efficiency is achieved for the propulsive system, the velocity deficit in the far wake is fully recovered between two jet peaks.

ACKNOWLEDGMENTS

The authors are grateful for the financial support from the National Natural Science Foundation of China (Nos. 51278297 and 51679139) and the Major Program of the National Natural Science Foundation of China (No. 51490674), Research Program of Shanghai Leader Talent (No. 20) and Doctoral Disciplinary Special Research Project of Chinese Ministry of Education (No. 20130073110096). Y.B. also likes to acknowledge the financial support from Shanghai Natural Science Foundation under Grant No. 17ZR1415100.

[1] Agrawal, A., Djenidi, L., and Antonia, R. A., "Investigation of flow around a pair of side-by-side square cylinders using the lattice boltzmann method," Comput. Fluids **35**(10), 1093–1107 (2006).

[2] Anderson, J. M., Streitlien, K., Barrett, D. S., and Triantafyllou, M. S., "Oscillating foils of high propulsive efficiency," J. Fluid Mech. **360**, 41–72 (1998).

[3] Ashraf, I., Agrawal, A., Majid, H., Sooraj, P., Atul, S., and Atul, S., "Thrust generation and wake structure for flow across a pitching airfoil at low Reynolds number," Sadhana **40**, 2367–2379 (2015).

[4]Bao, Y. and Tao, J. J., "Dynamic reactions of a free-pitching foil to the reverse karman vortices," Phys. Fluids **26**, 031704 (2014).
[5]Bao, Y., Zhou, D., and Tu, J., "Flow interference between a stationary cylinder and an elastically mounted cylinder arranged in proximity," J. Fluids Struct. **27**(8), 1425–1446 (2011).
[6]Bao, Y., Huang, C., Zhou, D., Tu, J., and Han, Z., "Two-degree-of-freedom flow-induced vibrations on isolated and tandem cylinders with varying natural frequency ratios," J. Fluids Struct. **35**, 50–75 (2012).
[7]Bao, Y., Zhou, D., and Tu, J., "Flow characteristics of two in-phase oscillating cylinders in side-by-side arrangement," Comput. Fluids **71**, 124–145 (2013).
[8]Bao, Y., Zhou, D., and Huang, C., "Numerical simulation of flow over three circular cylinders in equilateral arrangements at low Reynolds number by a second-order characteristic-based split finite element method," Comput. Fluids **39**(5), 882–899 (2010).
[9]Blackburn, H. M. and Ron, D. H., "A study of two-dimensional flow past an oscillating cylinder," J. Fluid Mech. **385**, 255–286 (1999).
[10]Burattini, P. and Agrawal, A., "Wake interaction between two side-by-side square cylinders in channel flow," Comput. Fluids **77**, 134–142 (2013).
[11]Carini, M., Giannetti, F., and Auteri, F., "On the origin of the flip–flop instability of two side-by-side cylinder wakes," J. Fluid Mech. **742**, 552–576 (2014).
[12]Codina, R. and Blasco, J., "Stabilized finite element method for the transient Navier–Stokes equations based on a pressure gradient projection," Comput. Methods Appl. Mech. Eng. **182**(3), 277–300 (2000).
[13]Codina, R., Blasco, J., Buscaglia, G. C., and Huerta, A., "Implementation of a stabilized finite element formulation for the incompressible Navier–Stokes equations based on a pressure gradient projection," Int. J. Numer. Methods Fluids **37**(4), 419–444 (2001).
[14]Deng, J., Sun, L. P., Teng, L. B., Pan, D. Y., and Shao, X. M., "The correlation between wake transition and propulsive efficiency of a flapping foil: A numerical study," Phys. Fluids **28**, 094101 (2016).
[15]Dewey, P. A., Quinn, D. B., Boschitsch, B. M., and Smits, A. J., "Propulsive performance of unsteady tandem hydrofoils in a side-by-side configuration," Phys. Fluids **26**, 041903 (2014).
[16]Dickinson, M. H. and Gotz, K. G., "Unsteady aerodynamic performance of model wings at low Reynolds numbers," J. Exp. Biol. **174**(1), 45–64 (1993).
[17]Donea, J., Giuliani, S., and Jean-Pierre, H., "An arbitrary lagrangian-eulerian finite element method for transient dynamic fluid-structure interactions," Comput. Methods Appl. Mech. Eng. **33**, 689–723 (1982).
[18]Dong, G.-J. and Lu, X.-Y., "Characteristics of flow over traveling wavy foils in a side-by-side arrangement," Phys. Fluids **19**(5), 057107 (2007).
[19]Godoy-Diana, R., Aider, J.-L., and Wesfreid, J. E., "Transitions in the wake of a flapping foil," Phys. Rev. E **77**(1), 016308 (2008).
[20]Godoy-Diana, R., Marais, C., Aider, J.-L., and Wesfreid, J. E., "A model for the symmetry breaking of the reverse Bénard–von Kármán vortex street produced by a flapping foil," J. Fluid Mech. **622**, 23–32 (2009).
[21]Griffin, O. M. and Ramberg, S. E., "The vortex-street wakes of vibrating cylinders," J. Fluid Mech. **66**, 533–576 (1974).
[22]Han, Z., Zhou, D., He, T., Tu, J. H., Li, C. X., Kwok, K. C. S., and Fang, C., "Flow-induced vibrations of four circular cylinders with square arrangement at low Reynolds numbers," Ocean Eng. **96**, 21–33 (2015).
[23]Hughes, T., Liu, W., and Zimmermann, T., "Lagrangian-Eulerian finite element formulation for incompressible viscous flows," Comput. Methods Appl. Mech. Eng. **29**, 329–349 (1981).
[24]Jones, K. D., Dohring, C. M., and Platzer, M. F., "Experimental and computational investigation of the Knoller-Betz effect," AIAA J. **36**(7), 1240–1246 (1998).
[25]Kang, S., "Characteristics of flow over two circular cylinders in a side-by-side arrangement at low Reynolds numbers," Phys. Fluids **15**(9), 2486–2498 (2003).
[26]Kaya, M., Tuncer, I. H., Jones, K. D., and Platzer, M. F., "Optimization of flapping motion parameters for two airfoils in a biplane configuration," J. Aircr. **46**(2), 583–592 (2009).
[27]Kumar, S. R., Sharma, A., and Agrawal, A., "Simulation of flow around a row of square cylinders," J. Fluid Mech. **606**, 369–397 (2008).
[28]Lai, J. C. S. and Platzer, M. F., "Jet characteristics of a plunging airfoil," AIAA J. **37**(12), 1529–1537 (1999).
[29]Lewin, G. C. and Haj-Hariri, H., "Modelling thrust generation of a two-dimensional heaving airfoil in a viscous flow," J. Fluid Mech. **492**, 339–362 (2003).
[30]Miao, J.-M., Sun, W.-H., and Tai, C.-H., "Numerical analysis on aerodynamic force generation of biplane counter-flapping flexible airfoils," J. Aircr. **46**(5), 1785–1794 (2009).
[31]Mizushima, J. and Ino, Y., "Stability of flows past a pair of circular cylinders in a side-by-side arrangement," J. Fluid Mech. **595**, 491 (2008).
[32]Schnipper, T., Andersen, A., and Bohr, T., "Vortex wakes of a flapping foil," J. Fluid Mech. **633**, 411–423 (2009).
[33]Shrivastava, M., Malushte, M., Agrawal, A., and Sharma, A., "CFD Study on Hydrodynamics of Three Fish-Like Undulating Hydrofoils in Side-by-Side Arrangement," in *Fluid Mechanics and Fluid Power - Contemporary Research* (Springer, 2017), pp. 1443–1451.
[34]Tay, W. B., Bijl, H., and van Oudheusden, B. W., "Biplane and tail effects in flapping flight," AIAA J. **51**(9), 2133–2146 (2013).
[35]Triantafyllou, G. S., Triantafyllou, M. S., and Grosenbaugh, M. A., "Optimal thrust development in oscillating foils with application to fish propulsion," J. Fluids Struct. **7**(2), 205–224 (1993).
[36]Triantafyllou, M. S., Triantafyllou, G. S., and Gopalkrishnan, R., "Wake mechanics for thrust generation in oscillating foils," Phys. Fluids A **3**(12), 2835–2837 (1991).
[37]Tu, J., Zhou, D., Bao, Y., Han, Z., and Li, R., "Flow characteristics and flow-induced forces of a stationary and rotating triangular cylinder with different incidence angles at low Reynolds numbers," J. Fluids Struct. **45**, 107–123 (2014).
[38]Tuncer, I. H. and Kaya, M., "Thrust generation caused by flapping airfoils in a biplane configuration," J. Aircr. **40**(3), 509–515 (2003).
[39]Weihs, D., "Hydromechanics of fish schooling," Nature **241**, 290–291 (1973).
[40]Williamson, C. H. K. and Roshko, A., "Vortex formation in the wake of an oscillating cylinder," J. Fluids Struct. **2**(4), 355–381 (1988).
[41]Zhang, X. P., Zhou, D., and Bao, Y., "Mesh motion approach based on spring analogy method for unstructured meshes," J. Shanghai Jiaotong Univ. (Sci.) **15**, 138–146 (2010).
[42]Zheng, Z. C. and Wei, Z., "Study of mechanisms and factors that influence the formation of vortical wake of a heaving airfoil," Phys. Fluids **24**(10), 103601 (2012).
[43]Zheng, Z. C. and Wei, Z., "Mechanisms of wake deflection angle change behind a heaving airfoil," J. Fluids Struct. **48**, 1–13 (2014).
[44]Zhu, Q. and Peng, Z., "Mode coupling and flow energy harvesting by a flapping foil," Phys. Fluids **21**, 033601 (2009).